Forschungszentrum Karlsruhe
Technik und Umwelt

Wissenschaftliche Berichte
FZKA 5834

Neutrino Flux Calculations for the Proposed European Spallation Source

R. L. Burman, P. Plischke
Institut für Kernphysik

November 1996

Forschungszentrum Karlsruhe
Technik und Umwelt

Wissenschaftliche Berichte
FZKA 5834

Neutrino Flux Calculations for the proposed European Spallation Source

R. L. Burman[1,*] and P. Plischke[**]
Institut für Kernphysik

[1] *Permanent address: P-Division, Los Alamos National Laboratory, Los Alamos, New Mexico 87545, USA.*

Forschungszentrum Karlsruhe GmbH, Karlsruhe
1996

Forschungszentrum Karlsruhe GmbH
Postfach 3640, 76021 Karlsruhe

ISSN 0947-8620

Abstract

The neutrino production rates for a spallation neutron source with proton beams in the energy range $650 < T_p < 2200$ MeV are calculated to an accuracy of 25%. The target geometries used are based upon the tantalum and mercury targets proposed for the European Spallation Source (ESS). Results for ν_μ, ν_e, and $\overline{\nu}_\mu$ rates due to π^+ and μ^+ decay at rest, and for ν_μ rates from π^+ decay in flight, are presented in terms of neutrinos per proton. For the ESS proposed energy of 1334 MeV and a tantalum target, the production rates for decay at rest are calculated to be $(\nu\ \mathrm{p}^{-1}) = 0.139$. For a neutrino detector located 20 meters away from the tantalum target, and at 0^o, the integrated flux of ν_μ above 150 MeV from π^+ decay-in-flight is 2.8×10^5 $(\mathrm{cm}^{-2}\ \mathrm{s}^{-1})$. Backgrounds of $\overline{\nu}_e$, from the π^- decay-in-flight and μ^- decay-at-rest chain, are found to be 0.08% of the ν_e flux.

* *e-mail:* *burman@lampf.lanl.gov*
** *e-mail:* *peter@ik1.fzk.de*

Berechnung der Neutrinoflüsse für die vorgeschlagene Europäische Spallationsneutronenquelle

Zusammenfassung

Die Produktionsraten von Neutrinos aus einer Spallationsneutronenquelle werden berechnet für Energien des Protonenstrahls im Bereich $650 < T_p < 2200$ MeV mit einer Genauigkeit von 25%. Für die Target-Geometrie wurden die Tantal- und Quecksilber- Targets zugrunde gelegt, die für die Europäische Spallationsquelle (ESS) vorgeschlagen wurden. Ergebnisse für die ν_μ-, ν_e- und $\overline{\nu}_\mu$- Raten aus π^+- und μ^+-Zerfällen in Ruhe und für ν_μ-Raten aus dem π^+-Zerfall im Fluge werden angegeben als Anzahl der erzeugten Neutrinos pro Proton. Für die vorgeschlagene Energie der ESS von 1334 MeV ergibt sich mit einem Tantal-Target die Produktionsrate aus dem Zerfall in Ruhe zu jeweils $(\nu \quad p^{-1}) = 0.139$. Der integrierte Fluss von ν_μ oberhalb 150 MeV aus dem π^+-Zerfall im Fluge ist 2.8×10^5 cm^{-2} s^{-1} für einen Neutrino-Detektor in 20m Entfernung vom Tantal-Target unter 0^o zum Strahl. Der $\overline{\nu}_e$- Untergrund aus dem π^--Zerfall im Fluge mit anschliessendem μ^--Zerfall in Ruhe beträgt 0.08% des ν_e-Flusses.

Contents

1 Introduction

Four spallation neutron sources are presently in operation, with several more in various stages of construction or planning. Present spallation facilities are fed by proton accelerators with beams of 10-200 micro-amperes, and proton energies of 800 MeV. There are, however, ambitious plans for new facilities whose proton accelerators would be in the multi-milliampere range. Most new accelerator-fed spallation neutron projects will focus upon higher proton beam energies, typically 1-3 GeV, in order to improve neutron production per unit cost.

The proposed [1, 2] European Spallation Source (ESS) in its present conceptual design is based upon a 1.334 GeV linac. This linac would feed one or more storage rings that could be emptied in a single turn in order to provide short, and intense, pulses of protons. The expected total power in the proton beam would be 5 MW. When these protons interact in a massive tantalum or mercury target, neutrons are produced from spallation and fission processes. These neutrons would be moderated and used to provide an intense pulsed neutron source suitable for condensed matter studies.

In addition, the interaction of the proton beam in the tantalum or mercury target would produce a pulsed neutrino source of much higher intensities than presently available sources. Such a neutrino source would enable an exciting, and particularly timely, research effort in neutrino physics [3]. This report discusses Monte Carlo simulation of neutrino production by proton beams in the 1-2 GeV energy range and provides specific calculations for two possible ESS targets. Neutrino production rates are given for the ν_e, ν_μ and $\overline{\nu}_\mu$ beams from π^+ and μ^+ decay at rest, for the $\overline{\nu}_e$ backgrounds from μ^- decay at rest, and for the ν_μ beams from π^+ decay in flight. These rate estimates will be an important ingredient for the design of a neutrino facility and for the proposal of specific neutrino experiments.

The Monte Carlo code for the present study was initially designed[4] for lower energy proton beams. Measured cross sections for proton reactions, and for proton production of pions at proton energies of 585 and 730 MeV, were first parameterized. These parameterizations were incorporated into a Monte Carlo simulation of pion production in a thick target, followed by Monte Carlo tracking of pions and decay muons. A measurement of the stopped π^+ rate as a function of position within a thick target, for pions produced by protons of 700-800 MeV, was used for an absolute calibration[5] of the output from the computer code. This computer code has been used for neutrino production at 800 MeV proton accelerator beam stops and spallation targets and has been described in considerable detail[4, 6, 7]. For that reason we will only present in this report those additions to the code that enable studies of neutrino production at higher energies.

Calculations and parameterizations of pion production cross sections are given in Sec. 2, with the detailed algorithms relegated to the Appendix. The modifications to the neutrino production computer code are discussed in Sec. 3, and the modelling of the ESS target described in Sec. 4. Neutrino flux computations and the results are discussed in Sec. 5 for pion and muon decay at rest and for pion decay in flight. Sec. 6

contains a summary and recommendations.

2 Pion production by GeV protons

At 1.5 GeV about 60% of the incident protons produce a pion in interactions within a spallation target. The charged pions produced in a tantalum or mercury target stop very quickly (< 3 ns) because of their relatively low energies (~ 200 MeV), and because of the high stopping power of the target material, so that most of the π^+ decay at rest. Because the pion has spin 0, both the μ^+ and the associated 30 MeV ν_μ are emitted isotropically. The π^+ decay at rest is followed by the μ^+ decay within 0.2 g/cm^2 of the point at which the π^+ stopped, as the muon kinetic energy is 4.1 MeV. Again, because of the isotropic distribution of muon momenta, the 0-53 MeV $\overline{\nu}_\mu$ and ν_e fluxes are isotropic. The majority of the pions decay in the immediate vicinity of their production point, and thus a neutron spallation facility represents an extremely intense, approximately point-like, source[8] of neutrinos for nuclear and particle physics studies.

The produced π^- which stop are all absorbed by nuclei. No neutrinos are emitted in this process. It is the 1% of produced π^- that decay in flight, and the fraction of resulting μ^- that decay at rest rather than capture, that would lead to a $\overline{\nu}_e$ background for several possible experiments.

A higher energy ν_μ beam, extending beyond 250 MeV, results from the decay in flight of π^+. For neutrino detectors located directly downstream of the spallation target, these ν_μ beams are of sufficient intensity to present opportunities for yet additional neutrino experiments.

2.1 Cross section calculations

The measured pion production cross sections at 730 and 585 MeV [9] cover a reasonable range of nuclei and a reasonable part of the pion energy-angle phase space. Above 730 MeV, however, there is a paucity of published data. Therefore we resorted to a calculation of pion production cross sections, and then normalized the calculated cross sections to the 730 and 585 MeV data.

The calculations were based upon the intra-nuclear cascade model of Bertini[10]. This model uses the extensive store of nucleon-nucleon data to produce energetic outgoing particles from complex nuclei by initial cascade reactions. [1] The cascade model includes both single and double pion production, e.g. $pp \rightarrow \pi^+ pn$ and $pp \rightarrow \pi^+\pi^+ nn$. Both of these processes should be important for proton energies above 1000 MeV.

A particularly convenient package of Monte Carlo computer codes for nucleon-induced reactions, the LAHET system[11] from the Los Alamos National Laboratory, which incorporates the Bertini model, was used for the calculations. Doubly-differential (in pion

[1] Lower-energy particles arise from evaporation, but that is not relevant to the present calculations.

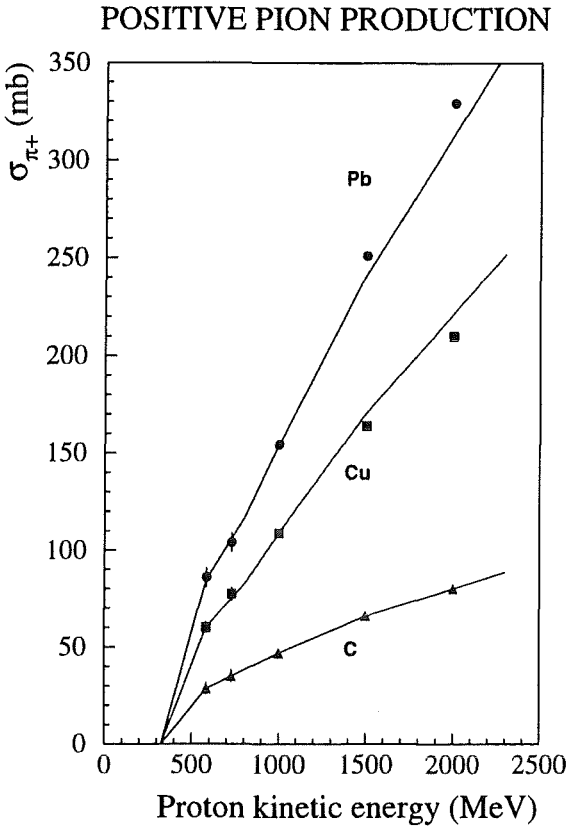

Figure 1: The total π^+ production cross sections, $\sigma_{\pi+}$, for carbon, copper and lead as functions of the proton energy T_π. A simple piece-wise linear energy dependence is assumed, with $\sigma_{\pi+}$ decreasing to zero at 325 MeV.

energy and angle) and total cross sections were computed for hydrogen, carbon, copper and lead at incident proton energies of 800, 1000, 1500 and 2000 MeV.

2.2 Total cross sections

As has been known for many years, the intra-nuclear cascade model, although the best currently available calculational tool, overestimates pion production. The calculated total cross sections, $\sigma_{\pi+}$ and $\sigma_{\pi-}$, are typically twice the measured values, at, e.g. 730 MeV. The reason for the over-calculation is presumably due to nuclear structure effects: for example, (a) large binding energies might cause nucleons in lower shells in the nucleus to be much less effective in pion production, and (b) quantum shadowing might be much stronger than geometrical shadowing.

In the pre-existing neutrino production computer code[4, 6] cross sections up to 800 MeV are generated by linear extrapolation of the measured cross sections at 585 and 730 MeV. Comparison of LAHET calculations made at 800 MeV to the extrapolations

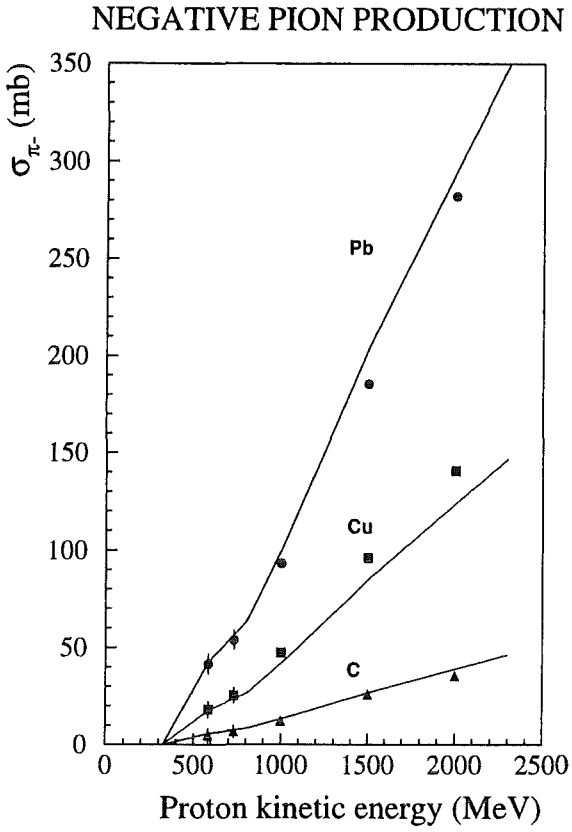

Figure 2: The total π^- production cross sections, σ_{π^-} , for carbon, copper and lead as functions of the proton energy T_π. A simple piece-wise linear energy dependence is assumed, with σ_{π^-} decreasing to zero at 325 MeV.

in the existing code showed the calculations to be too high by, e.g., factors of 1.52 for σ_{π^+} on carbon and 1.96 for σ_{π^+} on lead. All the LAHET calculated total pion-production cross sections were then normalized to the 800 MeV values by the respective factors. The resulting total cross sections for pion production from carbon, copper and lead are shown in Figures 1 and 2. The points at 585 and 730 MeV are the measured data, the points at 1000, 1500 and 2000 MeV are the (normalized) LAHET calculations. The straight-line segments on the figures are the total cross section values used in the Monte Carlo code; they do not go through the LAHET points because they are an average of the carbon, copper and lead values, fit to a $Z^{1/3}$ dependence for π^+ production and $N^{2/3}$ dependence for π^- production. All pion production is assumed to start above a proton energy of 325 MeV. The kinks at 800 MeV in the cross sections, for both π^+ and π^- production, arise from a differing slope in the LAHET (Bertini model) calculations and in the 585-730 MeV linear extrapolation in the Monte Carlo code. Details of the algebraic forms used for the total production cross sections are given in the Appendix.

Comparison of σ_{π^-} and σ_{π^+} for lead in Figures 1 and 2 shows that the π^- production cross section is approximately the same as that for π^+ by proton energies of 2000 MeV. This implies a larger background of $\overline{\nu}_e$ from μ^- decay at rest, as is made evident in Sec. 5.

2.3 Differential cross sections

Differential cross sections for pion production were produced from the LAHET code as functions of pion kinetic energy (T_π) and angle (θ_π). Examples of the calculated doubly-differential cross sections are shown, for lead, in Figures 3 and 4. The Monte Carlo simulation utilizes integral probability distribution tables, in T_π and θ_π, in order to select kinematical variables for the produced pions. In order to produce these tables, it is necessary to have the doubly-differential cross sections for each of the materials in the spallation target. This requirement is most easily met by parameterizing the calculated cross sections.

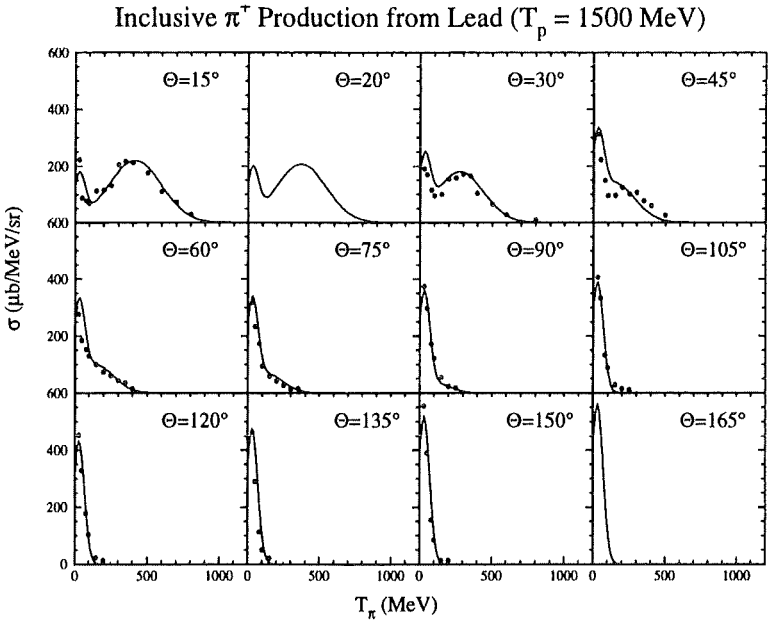

Figure 3: Comparison of the modelled π^+ production doubly-differential cross section (solid line) for lead at 1500 MeV proton energy with the LAHET calculations. The parameterization is that of eq. (1).

Inspection of Figures 3 and 4 suggest that there are two reaction channels dominating pion production in the 1-2 GeV range. The calculated points for both π^+ and π^- production exhibit two clusters, one with a peak at around 50 MeV and the secound

peaking at 300-400 MeV. The first cluster persists at all angles, being larger ($\times$ 2) at back angles; the second forms the bulk of the cross section at small angles but disappears beyond 90°. It is likely that the first cluster is due to multiple pion production, and the second to a direct, peripheral-type, reaction.

From the calculated values as a function of T_π in Fig. 3, it is evident that a functional form consisting of two exponential terms is sufficient. A procedure similar to that used for the previous modelling of π^- production[7] is followed. The dependence upon pion kinetic energy T_π is conveniently defined, for a given material Z and proton kinetic energy T_p, in terms of a sum of Gaussian forms:

$$\frac{d^2\sigma}{d\Omega_\pi dT_\pi} = \left[A_1 e^{-\left(\frac{\overline{T}_1 - T_\pi}{\sqrt{2}\sigma_1}\right)^2} + A_2 e^{-\left(\frac{\overline{T}_2 - T_\pi}{\sqrt{2}\sigma_2}\right)^2} \right] \times \left(1 + e^{\frac{T_\pi - T_F}{B}}\right)^{-1}. \qquad (1)$$

The functional dependence on T_π is simple, it appears only in the exponents of the Gaussians and in the high-energy cut-off factor. This latter factor, the last term in eq. (1), is employed to produce a smoothed form of energy conservation, $T_F = T_p - 140$ MeV $- 2B$. The sharpness of the cut-off is determined by the parameter B, set to 25 MeV.

The parameters A_i, $\overline{T}$ and σ_i were adjusted to give a reasonable fit to the points calculated from the LAHET code, and have a smooth dependence on Z. Simple piecewise-continuous analytical forms suffice for the dependence of these parameters upon Z, T_p, and θ_π; the detailed functional forms are given in the Appendix. Comparison in Figures 3 and 4 of the functional forms (solid lines), and the LAHET calculations (points), shows that the form of Eq. 1 adequately reproduces the calculations.

Although the pion production total cross sections $\sigma_{\pi+}$ and $\sigma_{\pi-}$ are strongly dependent upon the incident proton energy T_p, the shapes of the doubly-differential cross sections have little dependence on T_p. We chose, therefore, to use the shapes at $T_p = 1500$ MeV for all proton energies above 800 MeV. It should be emphasized that only the shapes of $d^2\sigma/d\Omega_\pi dT_\pi$ enter the normalized integral probability distribution tables, and then only for the purpose of selecting outgoing pion kinematics; the actual probabilty of pion production comes from the total cross sections illustrated in Figures 1 and 2.

3 Modifications to the neutrino production code

The neutrino production code will continue to be extensively used, at 800 MeV, for calculations of neutrino fluxes for the KARMEN experiment at the Rutherford-Appleton Laboratory and for the LSND experiment at the Los Alamos National Laboratory. Because the code has an absolute normalization at proton energies T_p below 800 MeV, we prudently decided to leave this existing part of the Monte Carlo coding essentially untouched. Thus, for pion production above 800 MeV we have programmed additions, patches and some obvious duplications into the Monte Carlo code.

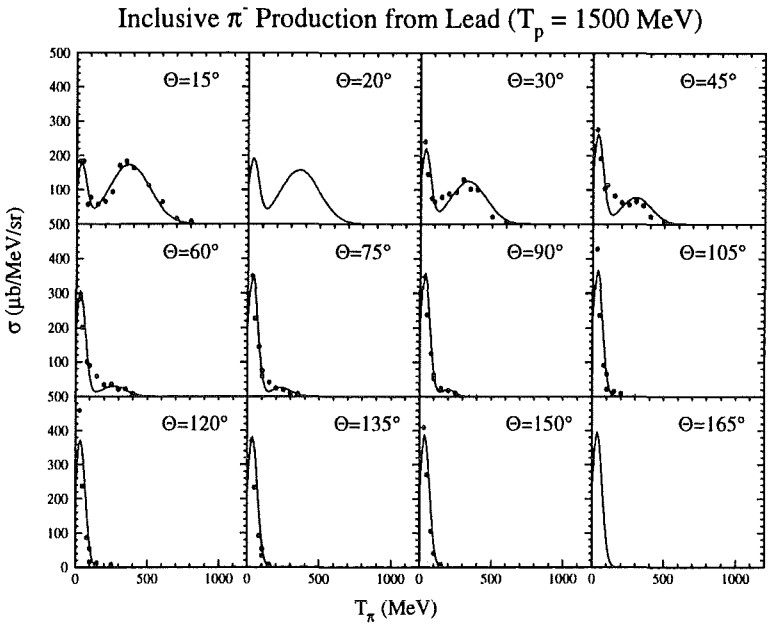

Figure 4: Comparison of the modelled π^- production doubly-differential cross section (solid line) for lead at 1500 MeV proton energy with the LAHET calculations. The parameterization is that of eq. (1).

For example, the integral probability distribution tables have been extended to cover the proton energy range $T_p > 800$ MeV. The probability distributions for the energy (T_π) and angle (θ_π) of the produced π^+ or π^- were generated through use of the doubly-differential cross section shapes, e.g., as shown for lead in Figures 3 and 4. This was done with a new set of tables in a new array, so that an entry into the tables for $T_p \leq 800$ MeV goes to the original array, and entries for $T_p > 800$ MeV go to the new array.

In all, modifications were made to the subroutines ipd, piabsorb, pimat, pint, pippi, pisig, pitot, sigpi, and setup; the functions of the subroutines are described in Table 1. Care was taken that, at each step in the installation of new coding, results from the code for incident energies $T_p < 800$ MeV were unchanged.

Routines for the computation of approximate range-energy relations for protons, pions and muons are used very frequently in the Monte Carlo code. A check showed that these routines still gave answers, at higher energies, that were within (1-3)% of the calculations in available tables based upon the Bethe-Bloch formulae.

At $T_p = 1500$ MeV, approximately 30% of the pions produced by the proton interactions are then absorbed in the various target materials before they can come to rest and

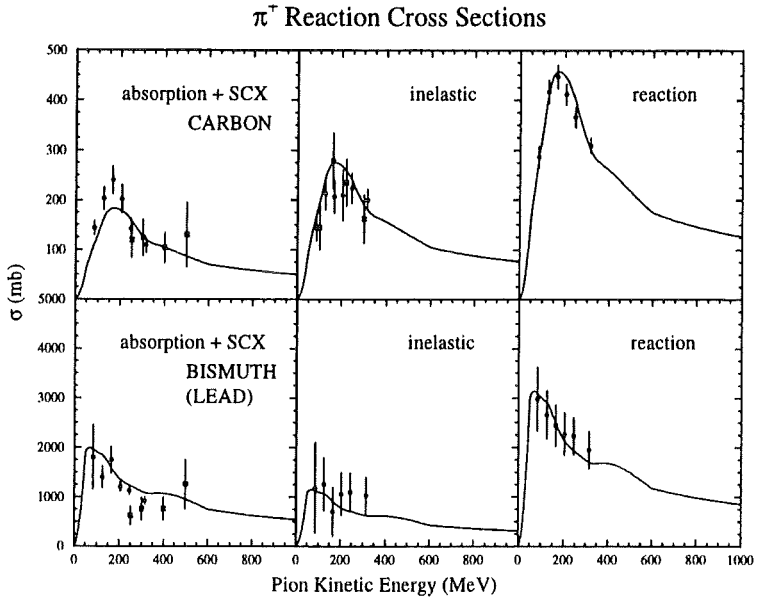

Figure 5: The cross sections for π^+ reactions in carbon and bismuth. The solid line is the algorithmic form used in the code, while the data is from ref[12, 13, 14]. The extensions to the code are the exponential tails starting at 600 MeV.

decay. It is thus important to model the pion reaction process, absorption and inelastic scattering, and include these reactions in the Monte Carlo code. There is little useful data, however, above 500 MeV. Instead, a "reasonable" extrapolation to 600 MeV was made in the original code[4]. This has been continued in the present expansion of the code, for $T_\pi > 600$ MeV, by a simple exponential tail. The shapes used are shown in Fig.5 for carbon and bismuth (or lead) as a function of T_π.

4 ESS target geometry

Geometry definition for the neutrino production Monte Carlo code is handled by the external geometry package used in the Los Alamos MCNP program[15]. This is a very versatile, well supported set of routines that allow the user to define cells in space and the materials that the cells enclose. The geometry package was neatly removed from the MCNP code, and incorporated into the neutrino production code.

A neutron spallation target facility consists of a spallation target assembly (in which the proton beam produces neutrons and pions), in close proximity to one or more neu-

Table 1: The subroutines in the neutrino production Monte Carlo code that were modified in order to allow computations for $T_p > 800$ MeV.

Subroutine	Task
ipd	Calculates integral probability tables for T_π and θ_π
piabsorb	Determines if pion is absorbed or scattered
pimat	Calculates σ_{π^-} and σ_{π^+} for given material and T_p
pint	Integrates $d^2\sigma/d\Omega_\pi dT_\pi$
pippi	Determines T_π and θ_π for given material and T_p
pisig	Calculates $d^2\sigma/d\Omega_\pi dT_\pi$ for Z, N and T_p
pitot	Calculates σ_{π^-} and σ_{π^+} for Z, N and T_p
sigpi	Calculates $d^2\sigma/d\Omega_\pi dT_\pi$ kernal for pisig
setup	Sets up materials as 1- or 2-molecule compounds, runs ipd

tron moderators, surrounded by a neutron reflector. The ISIS target facility has been modelled in some detail for neutrino production[6]. For ISIS, a spallation target assembly consisting of tantalum plates separated by cooling water is surrounded by a Be+water reflector; inside the reflector, just above and below the tantalum target assembly, are four neutron moderators and neutron channels.

For this report, the prospective ESS spallation targets were modelled as being similar to the ISIS target. The reflector assembly and target assembly were lengthened, in order to accomodate the higher energy incident proton beams. A vertical section, on the proton beam center line, of a spallation target composed of tantalum plates is shown in Fig. 6. The proton beam passes through a water cooled inconel beam window, and is stopped in a 70 cm target consisting of layers of thin disks of tantalum. Each disk is held in a square stainless steel retaining plate; the spaces between and surrounding the disks are filled with rapidly flowing heavy water as a coolant. This assembly of plates is held within a stainless steel pressure vessel, containing manifolds for heavy water coolant. The arrangement of the neutron moderators, with two above and two below the target, appears in Fig. 6.

For the mercury target, the inner section of the target assembly containing the plates and cooling manifolds was replaced with a solid rectangular box of mercury. [2] The liquid mercury is held in a steel can, closely surrounded by a water-cooled containment vessel.

[2]In the code, lead of density 13.3 is used to represent the liquid mercury; since the atomic number of mercury is 80 and that of lead 82, this use of lead is reasonable.

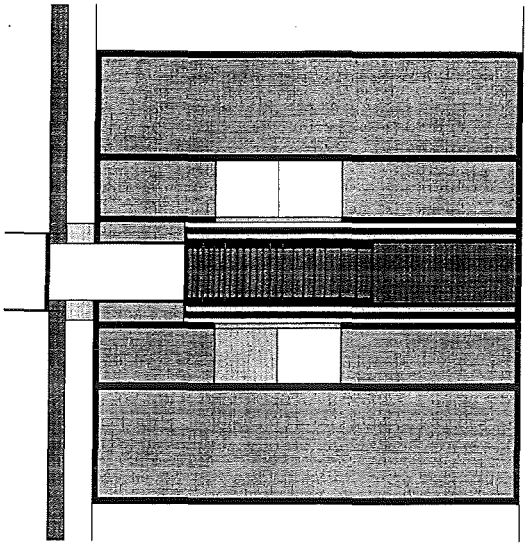

Figure 6: Vertical section of the ESS target geometry as modelled for a tantalum-plate design. Steel-jacketed water cooling channels are above and below the tantalum plates. Four neutron moderators, surrounded by a Be+water reflector, are shown with two above and two below the target. The proton beam is incident from the left, through a vacuum window.

5 Calculations, results, and disscussion

The neutrino production Monte Carlo code, with the modifications for use at higher incident proton energies as outlined above, was used for calculations of neutrino production at an ESS facility. Spallation target geometries for both tantalum and mercury cores, as described in Sec.4, were used in the calculations.

5.1 Neutrino production from pion and muon decay at rest

The decay-at-rest neutrino production, for proposed target materials (tantalum and mercury) in the present ESS proposal is given in Table 2. The incident proton energy of 1334 MeV is the design energy in the ESS proposal. Results are expressed as the number of π^+ and μ^+ decays at rest per incident proton for the given target configurations. In the last column the $\overline{\nu}_e$ background from μ^- decay at rest is given as a fraction of the number of π^+ and μ^+ decays at rest; the μ^- originate from π^- decays in flight. For the

Table 2: Calculated neutrino fluxes with the model tantalum and mercury targets for the proposed ESS facility. The incident proton energy of 1334 MeV is the current design specification. Column 3 gives the neutrino production from π^+ and μ^+ decays at rest in units of ν per proton, while column 4 gives the $\overline{\nu}_e$ background from μ^- decay at rest as a fraction of the number in column 3.

Spallation Target	Proton Energy (MeV)	Neutrino Flux ν_μ, ν_e, $\overline{\nu}_\mu$ (ν p^{-1})	Ratio $\overline{\nu}_e$ / ν_e (10^{-4})
Mercury	1334	0.127	8.0
Tantalum	1334	0.139	7.6
Tantalum + Pb reflector	1334	0.139	4.8

model target geometries chosen, the tantalum target has a 9% higher production rate than the mercury target. The $\overline{\nu}_e$ backgrounds for the two target materials, in the present state of the design, are similar, and actual predictions in any case will be very dependent upon the details of the spallation target construction. For example, it is possible that the normal reflector assembly of beryllium rods will be replaced by a lead reflector. The increased absorption of μ^- in lead would significantly reduce the $\overline{\nu}_e$ background, as is shown in the last row of Table 2.

The attraction of a facility like the ESS for neutrino research is apparent if we compare the projected neutrino flux to that for the present ISIS facility. At a beam power of 5 MW and energy of 1.334 GeV, the ESS accelerator beam intensity would be 3.75 milli-amperes. The ISIS facility presently operates at 800 MeV and 0.2 milli-amperes, so from Fig. 7 we find that the ratio of neutrino fluxes would be:

$$\nu(ESS)/\nu(ISIS) = (3.75/.2)(.139/.045) \approx 60 \qquad (2)$$

Neutrino cross sections are small, typically 10^{-40} cm^2, so that this large enhancement would greatly improve the accuracy of experiments, and in particular, would open areas of neutrino research that cannot be done now.

Calculations were also made for a range of incident proton beam energies, $650 < T_p < 2200$ MeV. The results, for both tantalum and mercury targets, are shown in Fig. 7. As noted above at $T_p = 1334$ MeV, the neutrino production per proton is slightly higher, as expected, for tantalum (Z=73) than for mercury (Z=80). In general, π^+ production will be higher for nuclei with a greater Z/N ratio.

For both targets the increase in neutrino production for proton energies above 800 MeV is dramatic, and is probably due to two phenomena: (1) At GeV energies the proton beam is well above threshold, and pion production is rising at least linearly. (Another way of expressing this effect is to note that the effective threshold for significant

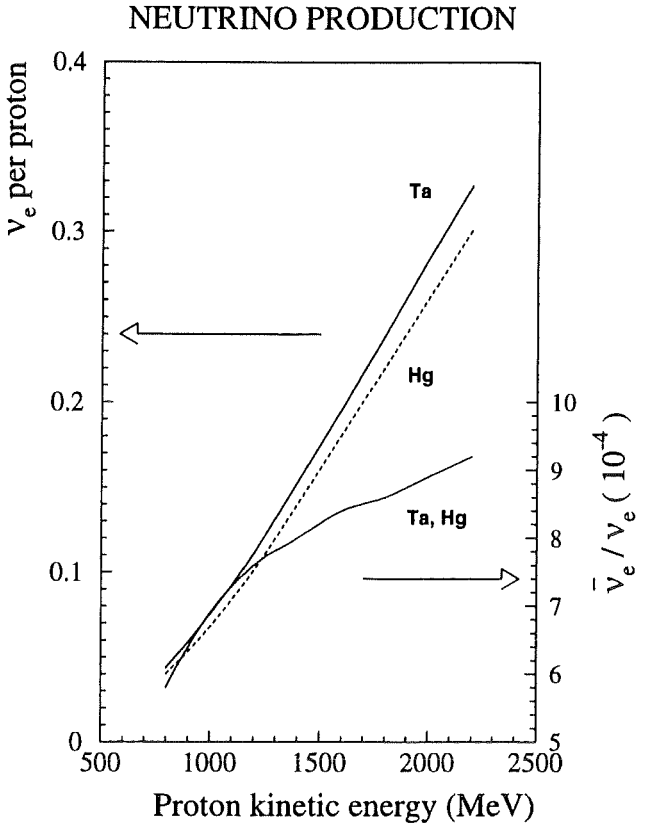

Figure 7: Neutrino production for ESS targets of tantalum and mercury as a function of incident proton energy. The number of ν_e , from π^+ decay at rest, are shown on the left axis. The ratio of $\overline{\nu}_e$ to ν_e , where the $\overline{\nu}_e$ arise from the decay at rest of μ^- throughout the spallation target assembly, is given on the right axis.

production of pions is around $T_p = 300$ MeV, so that the energy increase is relative to 300 MeV.) (2) At GeV energies multiple pion production, as recognized in Sec. 2.1, becomes important. Double pion production contracts the pion spectra to low energies, thus reducing the number absorbed in the target nuclei, and increasing the number that stop and decay at rest.

At the Los Alamos Meson Physics Facility a 20 cm water target, installed upstream of the copper beam stop, increased[4] the ν flux by 24%, because the higher proton/neutron ratio in water than in copper gives an enhanced π^+, and hence neutrino, production. This same concept, applied to a tantalum neutron spallation target with an 800 MeV proton source, would result in a 67% increase in neutrino production[16]. At 1-2 GeV proton beam energies, however, the improvement due to the addition of a low-Z target upstream of the main spallation target is calculated to be less important; in Fig. 8 we show calculations for an 8.0 cm block of aluminum replacing the first 8 cm section

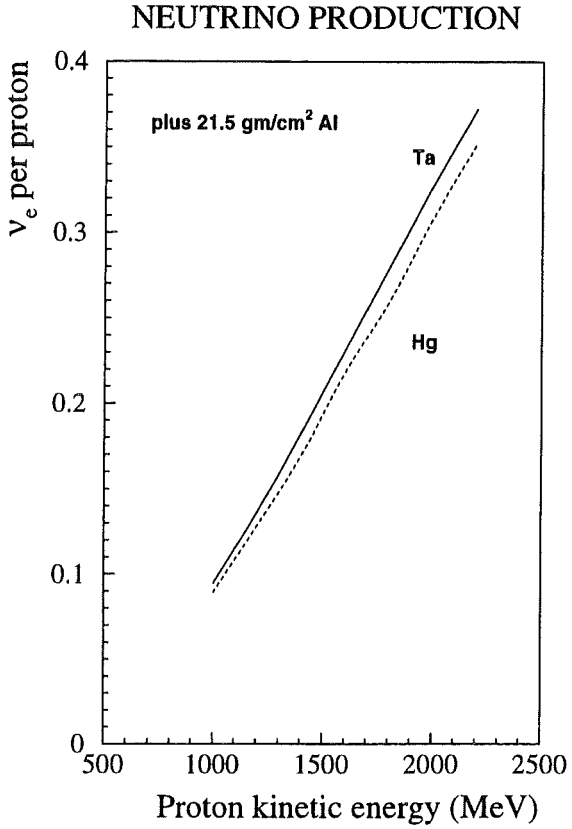

Figure 8: Neutrino production for ESS targets with an initial 8.0 cm aluminum block followed by a tantalum or mercury target. The number of ν_e , from π^+ decay at rest, are shown as a function of incident proton energy.

of tantalum plates or of mercury for the ESS target. The increase in ν per proton, compared to Fig. 7, ranges from 31% (1000 GeV) to 17% (2200 GeV) for a mercury target.

It is difficult to estimate the uncertainties in these calculations, because the accuracy of the pion production cross sections from the LAHET code are simply unknown. There are certainly additional nuclear effects that are important, beyond those incorporated into the Bertini intra-nuclear cascade model; indications of this are evident in a recent attempt[17] to reproduce pion inelastic scattering at T_π = 500 MeV. Judging from the normalization factors of 1.5 to 2 that are needed to make the calculated cross sections at T_p= 800 MeV agree with the extrapolations of the measured cross sections, we would estimate the uncertainty in the neutrino production rate to be about $\pm$25%.

Neutrino backgrounds of $\overline{\nu}_e$'s from μ^- decay at rest also increase with energy, as shown to the right of Fig. 7. This is because the π^- production cross sections for high-Z materials increase more rapidly with proton energy than do the π^+ cross sections.

The initial rapid rise in the $\overline{\nu}_e$ to ν_e ratio moderates above $T_p = 1200$ MeV, however, as the σ_{π^-} and σ_{π^+} cross sections increase at more nearly the same rate.

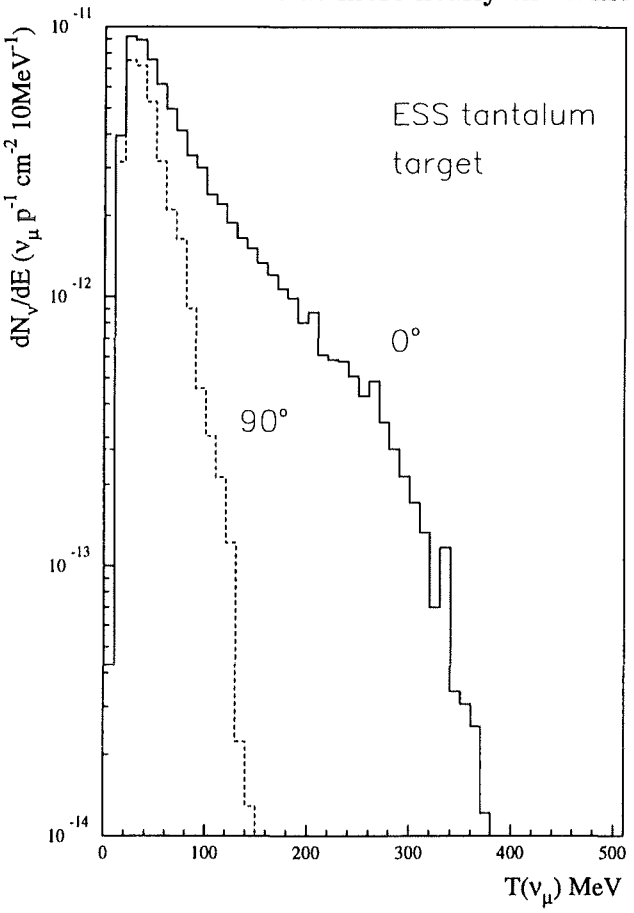

Figure 9: Muon-neutrino beam energy spectra from π^+ decay in flight. The solid curve is for a neutrino detector located 20 m from the ESS spallation target and at 0^o to the incident 1334 MeV proton beam; the dashed curve is for a detector at 90^o to the proton beam.

It is possible to use the sharp time structure in the proton beam of a neutron spallation source to reduce the effects of the $\overline{\nu}_e$ background. The $\overline{\nu}_e$ time spectrum actually consists of two basic components: (1) an exponential decay in low-Z materials like Be and D_2O dominated by the 2.2 μs muon mean life, and (2) the much faster exponential decay in high-Z materials Fe, Ta and Hg characterized by a fast absorption rate. If the neutrino reaction of interest is restricted to one of these time intervals, it is then possible to eliminate a portion of the background. In general the $\overline{\nu}_e$ background can be reduced by 30%; see Ref. [7] for the details of this argument.

5.2 Neutrino beams from pion decay in flight

A higher-energy ν_μ beam will occur due to the decay in flight of π^+. Although there are, purposefully, no empty-space decay regions in the core of a neutron spallation target, π^+ mesons can still decay in flight at a useful rate. The typical time for pions to slow down from 300 MeV to 100 MeV is several nano-seconds, long enough for approximately 1% of the pions to decay. Calculations were made for a 1334 MeV proton beam incident upon the ESS spallation target. Two plausible positions for a neutrino detector, located 20 m from the neutron spallation target, were used: the neutrino detector placed at 90^o to the direction of the incident proton beam, and directly downstream of the target at 0^o to the incident proton beam.

The energy spectra of the ν_μ beams from the calculations of π^+ decay in flight are shown in Fig. 9. As the spectra are quite similar for the tantalum and the mercury targets, we show results only for the tantalum target. The solid curve, for the neutrino detector located at 0^o, exhibits a hard neutrino spectrum extending to 300 MeV. From the dashed curve for the detector at 90^o one sees a much softer spectrum, extending barely to the (ν_μ, μ^-) threshold above 105 MeV.

Table 3: Calculated neutrino fluxes for π^+ decay in flight (DIF) and decay at rest (DAR). A proton beam of $T_p = 1334$ MeV is incident upon the tantalum ESS target; the detector is 20 m from the target, located at 0^o to the proton beam.

Threshold (MeV)	Source	Integral Flux (ν p^{-1} cm^{-2} $\times$ 10^{-11})
0	DAR	277.
0	DIF	7.18
100	DIF	2.36
150	DIF	1.24
200	DIF	0.63
250	DIF	0.29

In Table 3, we extract from Fig. 9 the integrated ν_μ flux, above a given threshold energy, for the neutrino detector located at 0^o. Because most experiments involving ν_μ neutrinos have a threshold above 105 MeV, we list in Table 3 several thresholds of possible interest from 100 to 250 MeV. The calculated fluxes are considerable, the integrated flux above 150 MeV from Table 3 predicting 2.8×10^5 ν_μ (cm^{-2} s^{-1}) for an ESS proton beam of 3.75 milli-amperes. For comparison, we also give in the first row the flux, from Table 2, for decay-at-rest neutrinos at a distance of 20 m from the target.

A gauge of the usefullness of the intensities produced is obtained from comparison to the decay-in-flight beam used in the LSND experiment at Los Alamos. From Fig. 9, one gets a flux at 200 MeV of approximately 8×10^{-14} ν_μ (p^{-1} cm^{-2} MeV^{-1}), to be compared to 4×10^{-14} ν_μ (p^{-1} cm^{-2} MeV^{-1}) used in the current LSND experiment

[18]. As the proton beam intensity at the ESS is expected to be about 5 times that used in the LSND experiment, the ESS decay-in-flight ν_μ beam would be a factor of 10 larger at 200 MeV, and a factor of 50 larger at 250 MeV. Such a neutrino flux would allow an expanded neutrino experimental program.

6 Summary and recommendations

Modifications to the KARMEN neutrino production code have been described, that enable calculations to be made for proton beams in the 1-2 GeV energy range. Pion production cross sections, calculated with the Bertini-model portion of the LAHET code package, were normalized, then parameterized and included as additions to the earlier neutrino production code. Pion tracking was extended to higher energies. The code modifications left results for incident energies $T_p < 800$ MeV unchanged.

Target geometries for two proposed ESS target structures, one based upon tantalum plates and one upon liquid mercury, were described. These geometries were used for calculations of neutrino production rates at a proton energy of $T_p = 1334$ MeV (the present ESS design specification) and for a range of energies $650 < T_p < 2200$ MeV. At $T_p = 1334$ MeV, the calculated neutrino production for the tantulum target is (ν p^{-1}) = 0.139, a considerable increase over the present value of 0.045 achieved at the 800 MeV ISIS facility. The predicted $\overline{\nu}_e$ background for the tantalum target is $\overline{\nu}_e$ / $\nu_e = 7.6 \times 10^{-4}$, somewhat larger than the present calculations for ISIS[6] of 6.2×10^{-4}.

If a neutrino detector were located at 0^o relative to the incident proton beam, there would also be available a ν_μ beam with a neutrino energy spectrum extending to 300 MeV. At the ESS this decay-in-flight ν_μ beam would be larger by factors of 10 to 50 than beams used to date, and could support additional neutrino experiments.

Although the neutrino production rates presented in this report, and the computer code upon which they are based, should prove useful both for design and assessment of a neutrino facility and for proposals for specific neutrino experiments, they are not accurate enough for analysis of the results from the eventual neutrino experiments. A neutrino research program, at a spallation source with proton energy well above 800 MeV, should have a comprehensive program to measure with precision the required pion production and transport cross sections, and to incorporate them into a new Monte Carlo code.

The measurements might include the following: (1) Reaction cross sections for protons (or neutrons) in the few hundred MeV to several GeV range, over a wide range of nuclei. Presently, these are not known to better than 10-15% accuracy; it would be preferable to have data with 5% accuracy. (2) Pion production cross sections, in doubly-differential form in energy and angle. Again, these should be done over a wide range of nuclei and preferably with accuracies of 5%. (3) Pion aborption, reaction and inelastic scattering cross sections on at least several nuclei from carbon to lead. The data that now exists has 20-40% accuracy. One would like better accuracy, but it should be recognized that these are difficult experiments. (4) An absolute calibration experiment, similar to

the "mock beam stop" experiment done at Los Alamos[5]. In this experiment, a 50 kHz proton beam interacted in an instrumented beam stop, consisting of slabs of material (water, copper and lead) interspersed with thin plastic scintillators. The scintillators recorded coincident pulses from the sequence of a stopping pion, a decay muon, and a decay electron. This data allowed the Monte Carlo code to be compared to stopped pion production throughout a thick target medium[4]. The experiment should be redone at energies from 800 MeV to 2000 MeV. Uncertainties on the earlier experiment dominate the neutrino flux errors at 800 MeV; a new calibration experiment could be done with much improved statistical and systematic errors.

A new Monte Carlo code, with improved simulation features as well as better parameterization, would be desireable. The present Monte Carlo code, normalized as described above, is accurate for proton beams of 700-800 MeV to $\pm$ 6.7%. With reasonable care and effort, a program of measurement as outlined above and of code developement, could result in accuracies of 2-3% for neutrino rates from π^+ and μ^+ decay at rest. The effort required would be justified by the ambitious neutrino research program possible at an ESS facility.

7 Acknowledgements

We are grateful to L. Daemen for his considerable help with the LAHET code. We wish to acknowledge helpful conversations with T. Broome on the ESS target design, and to thank G. Drexlin and B. Zeitnitz for initiating and encouraging this study. This work was supported in part by the Forschungszentrum Karlsruhe (Germany).

A Cross section algorithms

The algorithmic form of the doubly-differential π^+ and π^- production cross sections was introduced in Sec. 2.3. Without the high-energy cut-off factor, the dependence from Eq. 1 upon π^- energy T_π, for a given material Z and proton kinetic energy T_p, is:

$$\frac{d^2\sigma}{d\Omega_\pi dT_\pi} = \left[A_1 e^{-\left(\frac{\overline{T}_1 - T_\pi}{\sqrt{2}\sigma_1}\right)^2} + A_2 e^{-\left(\frac{\overline{T}_2 - T_\pi}{\sqrt{2}\sigma_2}\right)^2} \right]. \qquad \text{(A.1)}$$

The functional forms of the parameters $A_{1,2}$, $\overline{T}_{1,2}$ and $\sigma_{1,2}$ appearing in eq. (1) were combinations of simple piece-wise-continuous linear functions with, for $A_{1,2}$ respectively, powers of Z for π^+ production and N for π^- production. Parameters of the various functions were adjusted to approximate the cross sections calculated with the LAHET code.

For positive pion production, the amplitudes $A_{1,2}$ are expressed as functions of the pion angle θ for three ranges in Z in the form

$$A_{1,2} = f(Z)(a_{1,2}(\theta) + b_{1,2}(\theta) \times \theta), \tag{A.2}$$

$$f(Z) = \begin{cases} 1 & 1{=}Z \\ ((Z/6)^{1/3})(.62 + .063Z) & 1{<}\ Z\ {<}12 \\ (Z/82)^{1/3} & 12{\leq}\ Z \end{cases} \tag{A.3}$$

where absolute normalizations of the cross sections are suppressed for clarity. The second Gaussian term disappears beyond angles of 90°,

$$A_2 = 0.0, \qquad \theta > 90^o. \tag{A.4}$$

The coefficients $a_{1,2}(\theta)$ and $b_{1,2}(\theta)$ are given, for the same ranges in Z, in Table A.1.

Table A.1: Positive pion production. Z and θ dependence for the coefficients a_i and b_i.

Range in Z	$\theta \leq 75^o$		$\theta > 75^o$		$\theta \leq 60^o$		$\theta > 60^o$	
	a_1	b_1	a_1	b_1	a_2	b_2	a_2	b_2
Z=1	8.0	-.013	8.42	-.019	30.	-.42	11.	-.10
1< Z <12	10.	0.40	25.8	0.19	80.	-1.0	40.	-.33
12≤ Z	120.	2.40	87.0	2.86	260.	-2.67	240.	-2.33

The widths $\sigma_{1,2}$ and centroids $\overline{T}_{1,2}$ of the two Gaussian functions in Eq. A.1 show again the same dependence upon ranges in Z. Values of σ_1 and $\overline{T}_1$ are given in Table A.2, along with a parameter T_b that defines the θ dependence of $\overline{T}_2$. The θ dependence

Table A.2: Positive pion production. Z and θ dependence for the width σ_1, the centroid $\overline{T}_1$ and the parameter T_b.

Range in Z	σ_1	$\overline{T}_1$	T_b
Z=1	50.	250.	700.
1< Z <12	30.	50.	600.
12≤ Z	40.	30.	550.

of σ_2 and $\overline{T}_2$ are expressed as

$$\sigma_2 = 160. - 1.22 \times \theta \tag{A.5}$$

$$\overline{T}_2 = T_b + ((100 - T_b)/90) \times \theta. \tag{A.6}$$

For negative pion production, the amplitudes $A_{1,2}$ are again expressed as functions of θ, but now more simply as power-laws for all values of N, in the form

$$A_1 = (a_1(\theta) + b_1(\theta) \times \theta)(N/126)^{2/3}, \quad \text{(A.7)}$$

$$A_2 = \begin{cases} (a_2(\theta) + b_2(\theta) \times \theta)(N/126)^{1/2} & \theta \leq 90^o \\ 0.0 & \theta > 90^o \end{cases} \quad \text{(A.8)}$$

where absolute normalizations of the cross sections are suppressed for clarity. The coefficients $a_{1,2}(\theta)$ and $b_{1,2}(\theta)$ are given in Table A.3. For the two Gaussian functions

Table A.3: Negative pion production. Dependence upon θ for the coefficients a_i and b_i.

$\theta \leq 75^o$		$\theta > 75^o$		$\theta \leq 60^o$		$\theta > 60^o$	
a_1	b_1	a_1	b_1	a_2	b_2	a_2	b_2
120.0	3.067	314.5	0.476	220.0	-3.167	50.0	-0.333

of pion energy, T_π, in Eq. A.1, the widths $\sigma_{1,2}$ and centroids $\overline{T}_{1,2}$ for negative pion production have no Z or N dependence, but are given as simple linear functions of angle:

$$\sigma_1 = 35. \quad \text{(A.9)}$$

$$\sigma_2 = 160. - 1.22 \times \theta \quad \text{(A.10)}$$

$$\overline{T}_1 = 35. \quad \text{(A.11)}$$

$$\overline{T}_2 = 400. - 2.22 \times \theta. \quad \text{(A.12)}$$

References

[1] I.S.K. Gardner, H. Lengeler and G.H. Rees, editors, "Outline Design of the European Spallation Neutron Source", ESS Report ESS 95-30-M (1995).

[2] J. Finney, *et al.*, "Scientific Case for the European Spallation Source", to be published as a Rutherford-Appleton Laboratory report (1997).

[3] G. Drexlin, J. Kleinfeller, B. Zeitnitz and R. Maschuw, "NESS: Neutrinos at the European Spallation Source," in reference [2].

[4] R.L. Burman, M.E. Potter and E.S. Smith, Nucl. Instr. and Meth. A 291 (1990) 621.

[5] R.C. Allen, *et al.*, Nucl. Instr. and Methods **A284** (1989) 347.

[6] R.L. Burman, A.C. Dodd and P. Plischke, Nucl. Instr. and Meth. in Phys. Res. A 368 (1996) 416.

[7] R.L. Burman, A.C. Dodd and P. Plischke, Forschungszentrum Karlsruhe report, FZKA 5595 (July 1995).

[8] B. Zeitnitz, Prog. Part. Nucl. Phys. **13** (1985) 445; T.A. Gabriel, *et al.*, Kernforschungszentrum Karlsruhe report, KfK 3174 (1981).

[9] D.R.F. Cochran, *et al.*, Phys. Rev. **D6** (1972) 3085; J.F. Crawford, *et al.*, Phys. Rev. **C22**, (1980) 1184.

[10] Hugo W. Bertini, Phys. Rev. 188 (1969) 1711.

[11] R.E. Prael and H. Lichtenstein, The LAHET Code System, Los Alamos National Laboratory report LA-UR-89-30, (Sept. 1989). The Bertini model[10] was first widely available through the Oak Ridge National Laboratory code HETC, see T.A. Gabriel *et al.*, Oak Ridge National Laboratory report ORNL-TM-3319 (1970); the HETC code is now embodied in LAHET. The authors apologize for all these sequentially entombed acronyms, but that is modern life.

[12] D. Ashery, *et al.*, Phys. Rev. **C23** (1981) 2173.

[13] S.M. Levenson, *et al.*, Phys. Rev. **C28** (1983) 326.

[14] M.K. Jones, *et al.*, Phys. Rev. **C48** (1993) 2800.

[15] J.F. Breismeister, Editor, "MCNP - A general Monte Carlo code for neutron and photon transport," Los Alamos National Laboratory manual LA-7396-M, Rev. 2 (1986).

[16] R.L. Burman and L.L. Daemen, Nucl. Instr. and Meth. in Phys. Res. A 370 (1996) 335.

[17] Bao-An Li, Wolfgang Bauer and Che Ming Ko, Phys. Lett. **B382** (1996) 337.

[18] M. Albert, *et al.*, Phys. Rev. **C51** (1993) 2800.